An On-Chip Micromachined Test Structure to Study the Tribological Behavior of Deep-RIE MEMS Sidewall Surfaces

R. Ranga Reddy(ID) , Yuki Okamoto(ID) , *Student Member, IEEE*, and Yoshio Mita(ID) , *Member, IEEE*

Abstract—An on-chip micro-mechanical test structure is presented to investigate the tribological behavior of deep reactive ion etching (DRIE) sidewall surfaces of microelectromechanical systems (MEMS) devices. The proposed test structure is fabricated on silicon on insulator (SOI) wafer using a standard surface micromachine process. Test structure consists of two orthogonally placed electrostatic comb-drive actuators, one is used to align a contact with the friction surfaces under a certain normal load, and another one is used to generate the tangential motion on contacted sidewall surfaces. To assess the frictional behavior of DRIE sidewall surfaces, both static and dynamic friction coefficients were studied for different DRIE process parameters. Wear analysis was carried out to extract the performance and reliability of MEMS sidewall surfaces during their operation. From the experiment results, it is found that with the increment of normal load, the static friction coefficient exhibits a nonlinear dependence, and however, it has less effect on the dynamic friction coefficient. DRIE process parameters have a significant influence on static and dynamic friction coefficients, i.e., variation in asperity size changes the real contact area between the contact pairs during their operation. From the wear analysis, it is found that the friction coefficient was very high initial value, then it drops with each subsequent cycle for a few cycles and finally reaches steady-state value.

Index Terms—Friction, MEMS, DRIE, sidewall surfaces, static friction coefficient, dynamic friction coefficient, wear.

I. INTRODUCTION

MICROELECTROMECHANICAL systems (MEMS) refers to the emerging field of miniaturized machines fabricated in batch processes using deposition, lithography, and etching techniques mainly developed by the integrated circuit industry. With the ease of integration and miniaturization, MEMS devices have been employed in many commercial fields such as entertainment, communication, automation, and as well as strategic fields such as defense and space [1], [2]. With the increase in demand for more complex

and compact devices has prompted the development of prototypes of MEMS possessing contact-mode structures, such as microrelays, latches, micromotors, and microswitches [3]–[7]. However, the insufficient knowledge of tribological issues at contact sidewall surfaces on a micro-scale, MEMS devices that consist of components with sliding contact surfaces during their operation are not fully commercialized [8]–[12]. Friction and wear consider as crucial parameters that decide the reliability and lifespan of MEMS devices that contain contacting surfaces [13]–[15]. When the characteristic dimensions decrease from the macroscopic to the micrometer size, the associated surface-to-volume ratio becomes large, as a result, the effects of gravity become negligible as compared with adhesive and friction effects [16]. Due to the surface roughness effects, the contact occurs only at high asperities when two solid bodies brought each other, and thus, the real area of contact is only a small fraction of the apparent contact area [17]. On the other hand, well-developed theories and models for friction measurement at macroscale might not be directly applied to microscale because of its scaling effects [18], so it is vital to rebuilding a micro-tribology theory in which the size effect is concerned. As for movable MEMS devices, because the gaps of contact pairs are in the range of nanometer-scale, even zero, the influence of the frictional and adhesive forces between these contact pairs increases significantly, which can degrade both the performance and life of MEMS devices [19], [20]. Therefore, specially designed micro-instruments are needed to focus on tribology issues in MEMS devices for reliable long-term operation in different environments.

Over the years, various friction measurement techniques at both in-plane and out-of-plane sliding interfaces have been proposed [21]. Perhaps the most popular method is to scrape the tip of an atomic force microscope (AFM) or a scanning probe microscope (SPM) across the surface of a film and measure the normal and transverse forces by using the tip itself [22], [23]. However, AFM/SPM studies investigate the tribological characteristics of only single asperity contacts, while MEMS contact surfaces involve multiple asperities and surface force apparatus (SFA) studies investigate the tribological characteristics of atomically smooth surfaces while contacting MEMS surfaces have finite surface roughnesses [24], [25]. And also, due to the different processing environments to which the sidewall and in-plane surfaces are exposed during micromachining, they are expected to be

different, both topographically and chemically [26]. Therefore, a dedicated microinstrument is desirable to study the friction and wear of MEMS sidewall surfaces in which the material properties and morphological nature of the contact sidewall surfaces under tests are similar to those of actual MEMS devices.

To investigate the frictional characteristics on surface micromachined sidewall structures, various MEMS devices were reported in the previous research [27]–[37]. According to [30], frictional forces such as van der Waals forces and adhesion forces play a subordinate role in the case of two DRIE structured surfaces, where the typical etch ripple structure leads to roughness or ripple of several 100 nm. The dominant frictional resistance is due to the microforming of the asperity tips against each other. According to [32], the normal force on the contact pair has a greater influence on the static friction coefficient at the microscale. For all researched MEMS tribometers, the generation of the normal force and the measurement of the frictional force are implemented by means of integrated electrostatic tangential actuators. Based on the linear theory, the applied electrostatic forces are used to determine the acting electrostatic forces in the microsystem [38].

From the analysis of the prior art, it is clear that although there are numerous publications on MEMS tribometers for measuring friction characteristics on sidewall surface structures [27]–[37], their results do not allow for unambiguous conclusions. And also, the frictional properties of deep reactive ion etching (DRIE) silicon sidewall surfaces have not been thoroughly investigated, even though the DRIE process used widely for MEMS device fabrication. Therefore, dedicated test structures are necessary to perform measurements on the friction behavior with representative friction surfaces and normal forces, to obtain exact behavior of contact sidewall surfaces [39].

This paper presents an on-chip micromechanical test structure to investigate the tribological behavior of DRIE sidewall surfaces. Fabricating the test structures on the same chip of MEMS devices ensures that the material properties, chemical, and morphological nature of both surfaces are the same. An experimental study is carried out to extract the friction coefficients and its behavior with the consideration of different DRIE process parameters, i.e., with different asperities (scalloping) size on sidewall surfaces by varying etching cycle rate. The dependence of frictional behavior and wear of contact pairs on the number of operation cycles is investigated. This article is mainly focused on how to extract the tribological properties of any DRIE process sidewall surfaces with our simple test structure. The result of this research deepens the better understanding of the tribological behavior of DRIE sidewall surfaces of MEMS devices in real working conditions. Also, the extracted parameters from the microinstrument provide a new solution for the development of more complex, reliable microstructures with sliding or rolling interfaces.

II. TEST STRUCTURE DESIGN AND WORKING PRINCIPLE

The test structure used to investigate the friction properties on sidewall surfaces of Deep-RIE MEMS devices reported
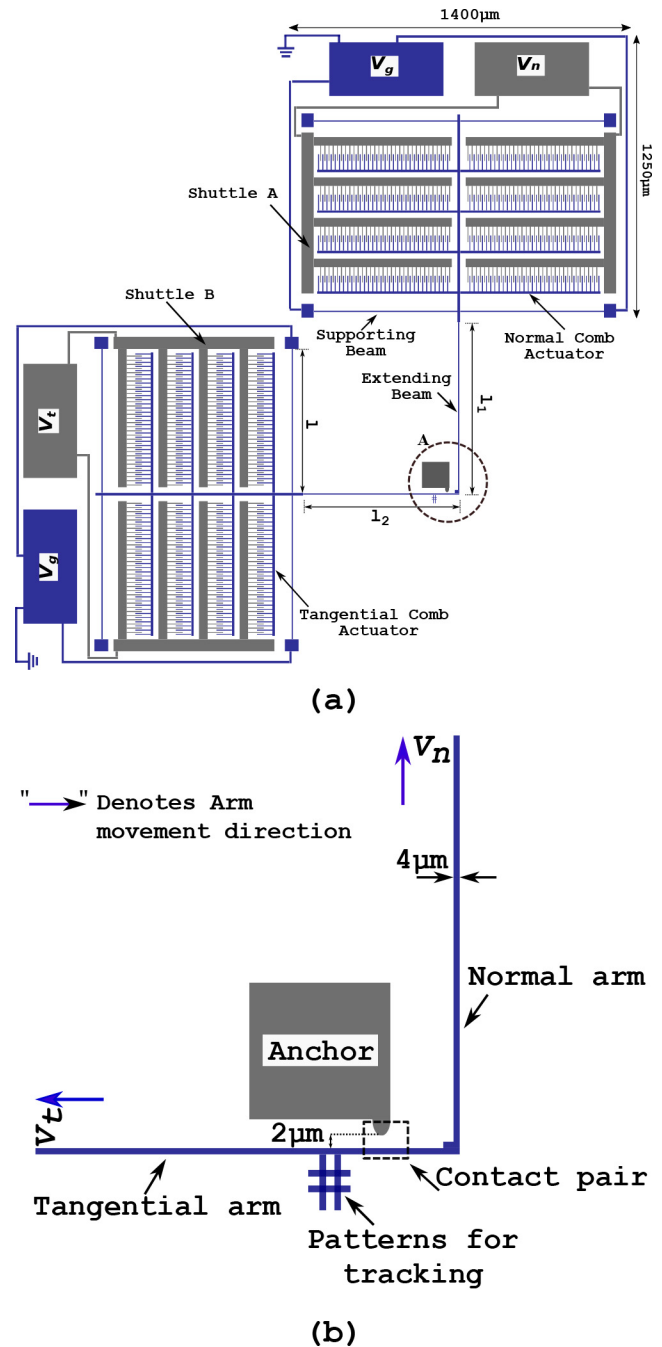

Fig. 1. (a) A schematic diagram of the proposed test structure used to study the tribological behavior on MEMS sidewall surfaces (b) Close up view of test structure with contact pairs and patterns for tracking the motion of contact pair during the experiment (enlargement of portion A).

in this article is inspired by the micro instrument developed by Ansari and Ashurst [36]. The schematic diagram of the proposed test structure for frictional analysis is shown in Fig. 1, and the close-up view of contacting structures with tracking patterns in the schematic is shown in Fig. 1b. The device consists of simple beam springs and two electrostatic comb-drive actuators integrated in such a way that they can produce motion in orthogonal directions. One of the comb actuators (normal arm) is used to form a contacting sidewall interface by bringing the flat sidewall surface of the flat beam
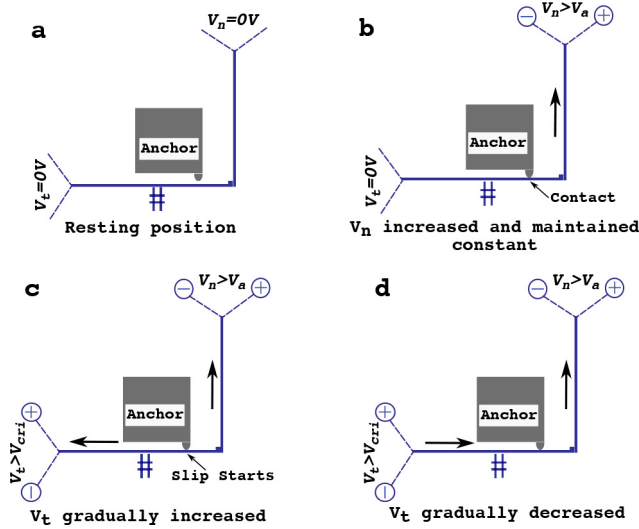
Fig. 2. A Schematic diagram of the test structure operation principle and its testing procedure (a) Normal and tangential arm at its initial state (b) Voltage on normal arm gradually increased to bring the sidewall surfaces into contact (c) Voltage on tangential arm increased by keeping voltage on normal arm constant to observe the forward motion on sidewall surfaces during contact (d) Voltage on tangential arm gradually decreased to observe the backward motion on sidewall surfaces during contact, where V_n = Voltage applied on a normal actuator, V_t = Voltage applied on a tangential actuator, $V_n = V_a$ = Voltage required to bring the sidewall surfaces into contact, $V_t = V_{cri}$ = Voltage at which slip starts between contact pair.

with the cylindrical sidewall on the anchor post surface. The contact sidewall interface is maintained at different normal loads by varying the voltage on the normal arm. The other comb actuator (tangential arm) is used to generate the tangential motion on the contacted sidewall surface once the normal arm has made contact. Each shuttle has extended beams in its movable part, supported by two pairs of suspended beams identically. The extended beams of these shuttles are 375 µm long, and 4 µm wide are connected perpendicularly, and supporting beams are 550 µm long and 4 µm wide. It is well known that, given the same actuation condition of the sliding component, the displacement amplitude is affected by the level of friction—the larger the friction is, the smaller is the amplitude. As a result, the friction force can be measured by detecting the variation of amplitude.

The schematic of the operating principle of the friction test structure is shown in Fig. 2. The initial gap between the contacting sidewall surfaces is designed 2 µm by considering the limitation of the fabrication process, and the contact sidewall surfaces are brought together by applying a DC voltage on the normal comb actuator (V_n). When the voltage on normal actuator $V_n = V_a$, the frictional pair (sidewall surfaces) is brought into contact, where V_a is the minimum voltage to bring those contact surfaces (Fig. 2b). After forming a sidewall interface, the voltage on the normal actuator increased first to induce a normal load on the contact surface, then the voltage on the tangential actuator (V_t) is increased step by step to generate tangential motion on contacted sidewall surfaces (Fig. 2c). At voltage $V_t = V_{cri}$, the electrostatic force on a tangential arm overcome the restoring force caused by the deflection of suspended beams of both tangential actuator and normal arm

and also the frictional force between the contact pair. During an experiment, the movement of the tangential arm is captured by the high-speed camera by varying the voltage V_t on tangential actuator under different normal load conditions on contact pairs. Image patterns are used to track the position of tangential arm for corresponding applied voltage to study the frictional behavior on contact pairs.

III. TEST STRUCTURE MODELLING AND TESTING PROCEDURE

Theoretical calculations are carried out during the design of the test structure and to predict the feasibility of the device. The relation between electrostatic force and driving voltages of shuttles, stiffness of test structure with frictional force and normal forces are all derived as mentioned below. During the operation, three electric potentials V_n, V_t, V_g, were applied. The ground potential, V_g, was applied to all the grounded parts of the components, a dc bias V_n, was applied to the normal comb actuator, and V_t, was applied to the tangential come actuator. According to the literature [38], by neglecting fringing effects, electrostatic force (F) generated by a comb drive actuator in the direction parallel to the comb fingers is given by

$$F = \frac{n\varepsilon t}{g} * V^2 \tag{1}$$

where n is the number of comb fingers on a comb drive actuator, ε is the dielectric constant of the material between the anchored and the suspended comb fingers (in this case, it is air), t is the thickness of comb fingers, g is the gap between the comb fingers, V is the driving voltage applied on the actuator. For simplicity, the constants are lumped into geometry parameter c. Therefore

$$c = \frac{n\varepsilon t}{g} \tag{2}$$

Accordingly,

$$F = cV^2 \tag{3}$$

The frictional test structures developed in this paper adopted two orthogonal comb-drive actuators to initiate the normal and tangential force on the contact sidewall surfaces, and to distinguish between them subscripts n and t are used for the normal and tangential arms, respectively. Accordingly

$$c_t = \frac{n\varepsilon t}{g_t} \tag{4}$$

$$c_n = \frac{n\varepsilon t}{g_n} \tag{5}$$

since the normal and tangential comb-drive actuators of test structure are identical to each other, therefore

$$c_t = c_n = c \tag{6}$$

combining equation (3) with the above equation gives

$$F_n = cV_n^2 \tag{7}$$

$$F_t = cV_t^2 \tag{8}$$

A specific driving voltage is applied on the normal arm to bring the loading beam in contact with anchor post, and the amount of force (F_a) required to bring the sidewall surfaces in contact is given by

$$F_a = \delta_a(k_n + k_{arm1}) = cV_a^2 \qquad (9)$$

where V_a is the voltage that is required to be applied on the normal comb actuator to bring the frictional pairs in to contact, k_n is the stiffness of suspended beams of normal comb actuator, k_{arm1} is the stiffness of extended beam (tangential arm) that connected to normal arm as shown in Fig. 1b, δ_a is the displacement of the normal arm to bring the frictional pair in to contact.

Using elastic beam theory, stiffness k_n and k_{arm1} can be expressed as

$$k_n = \frac{48EI}{l^3} \qquad (10)$$

$$k_{arm1} = \frac{12EI(l_1 + 3l_2)}{(4l_1 + 3l_2)l_2^3} \qquad (11)$$

where l is the length of the suspended beams, l_1 and l_2 are the length of the extending beams of a normal and tangential arm respectively, E is the elastic modulus of single-crystal silicon, I is moment of inertia of a single suspended beam, $I = \frac{hw^3}{12}$, w and h refer to the width and height of suspended beams in the bending direction.

In a separate measurement when the beam is not in contact with the anchor, electrostatic force (F_c) initiated by the tangential comb actuator must overcome the restoring force caused by the deflection of suspended beams of tangential actuator and extended beam (normal arm) that connected to the tangential arm and it is given by

$$F_c = \delta_c(k_t + k_{arm2}) = cV_c^2 \qquad (12)$$

$$k_{arm2} = \frac{12EI(l_2 + 3l_1)}{(4l_2 + 3l_1)l_1^3} \qquad (13)$$

where V_c is the voltage applied on the tangential comb actuator when friction pair is not in contact, k_t is the stiffness of suspended beams of tangential comb actuator, k_{arm2} is the stiffness of extended beam (normal arm) that connected to tangential arm as shown in Fig. 1b, δ_c is the displacement of a tangential arm when frictional pairs are not in contact.

The coefficient of static friction (μ_s) of the contacting sidewall surfaces can be determined using

$$\mu_s = \frac{F_t - F_c}{F_n - F_a} \qquad (14)$$

where F_n and F_t are the total tangential and normal forces generated at the instant of slip between the frictional pair using the normal and tangential comb actuators, respectively. Substituting equations (7), (8), (9) and (12) in the above equation gives

$$\mu_s = \frac{V_t^2 - V_c^2}{V_n^2 - V_a^2} \qquad (15)$$

Once the initiation of slip starts at the sidewall interface, the loading beam continues to slide with the anchor post until the sum of restoring force generated by the suspended beams of
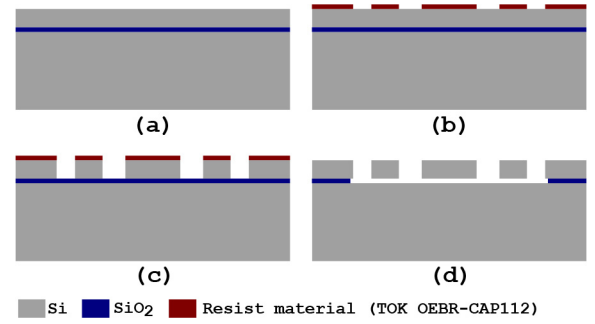

Fig. 3.   Schematic fabrication process flow of test structure (a) SOI wafer (b) Electron beam lithography (c) DRIE etching of Si layer (d) Sacrificial layer (SiO_2) release using Vapor HF Process.

a tangential arm and extended beams connects to normal arm and the dynamic friction force equal to the total force generated by the tangential comb actuator. Therefore, the coefficient of dynamic friction (μ_k) of contacting sidewall surface can be determined using

$$\mu_k = \frac{F_t - F_c - \delta_s(k_t + k_{arm2})}{F_n - F_a} \qquad (16)$$

where δ_s is the distance in which the loading beam slides on the contacting surface after its initiation. Substituting equations (7), (8), (9) and (12) in the above equation gives

$$\mu_k = \frac{V_t^2 - V_c^2 - \delta_s\left(\frac{k_t + k_{arm2}}{c}\right)}{V_n^2 - V_a^2} \qquad (17)$$

It should be noted that the additional normal load experienced by the sidewall interface due to adhesion between the contacting sidewall surfaces is not considered in equations (14) and (16). Therefore, the coefficients of friction are determined using equations (14) and (16) are engineering coefficients of friction.

IV. FABRICATION

The test structures were fabricated on silicon on insulator (SOI) substrate by using a standard surface micromachining process, as shown in Fig. 3. The SOI wafer, which was used to fabricate the test structure, consists of a 20 μm silicon device layer and a 2 μm silicon dioxide sacrificial layer on the silicon substrate of 625 μm. First, a 1.5-μm-thick EB resist (OEBR-CAP112 resist, TOK) was coated on SOI chip with 2500 rpm for 60 seconds and the designs were patterned using high-speed electron-beam lithography (F5112+VD01 EB writer, Advantest). Using patterned photoresist as an etching mask, deep reactive ion etching (DRIE) process was performed to etch the silicon device layer with MUC-21 ASE Pegasus (SPP Technologies). Since the etching step in the complete device fabrication process decides the sidewall profile, different DRIE process parameters were considered during fabrication and observed its influence on frictional properties. Bosch process was adopted for DRIE etching of the silicon device layer [40]. After the etching process, first, SOI chips were cleaned with, remover-104 (TOK), acetone, ethanol, to remove remaining EB resist. Then SOI chips are cleaned with $NH_4OH/H_2O_2/H_2O$ solution with a

TABLE I
DRIE PROCESS PARAMETERS USED FOR FRICTION TEST STRUCTURES

Process	Step	SF$_6$ flow rate (sscm)	C$_4$F$_8$ flow rate (sscm)	Process gas pressure (Pa)	Coil Power (W)	Bias Power (W)	Step time (sec)
DRIE-I	Passivation	–	150	3.5	1800	100	2
	Etching	300	–	4.5	1800	100	5
DRIE-II	Passivation	–	150	3.5	1800	120	1
	Etching	300	–	4.5	1800	120	1.5
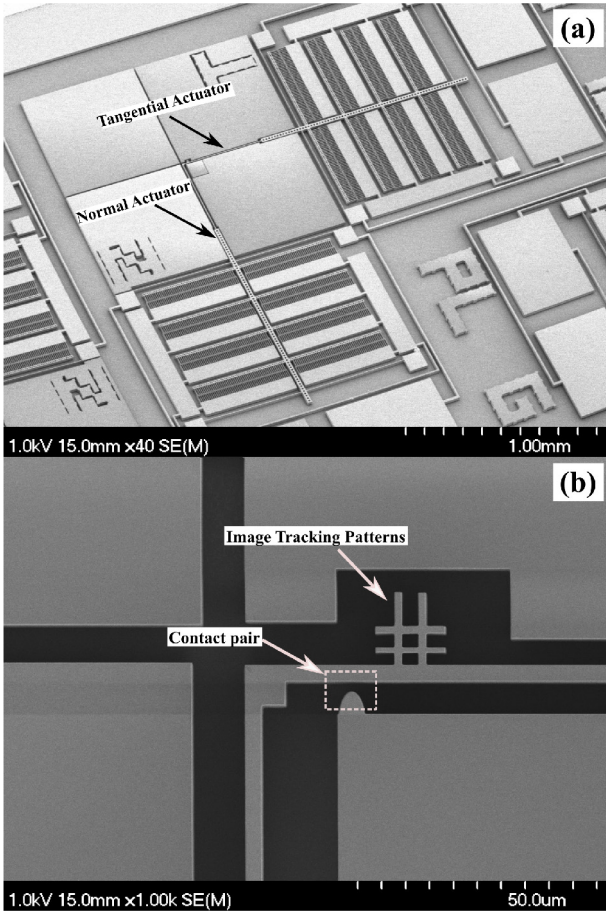
Fig. 4. (a) SEM image of fabricated test structure and (b) close up view of contact pair and tracking patterns used for measurements.
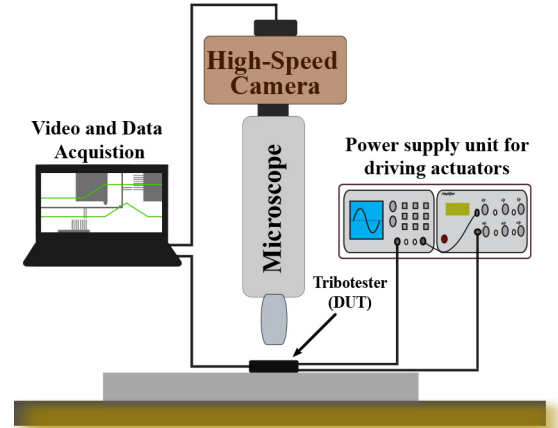

Fig. 5. Schematic diagram of experimental test setup used for friction analysis of DRIE sidewall test structures.
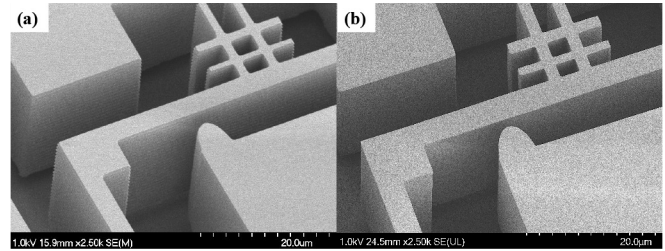

Fig. 6. Close up view of two DRIE test structure sidewall profile of contact surfaces (a) fabricated with DRIE-I process parameters (b) fabricated with DRIE-II process parameters.

ratio of 1/1/5 for 10 min at 80°C to remove residual Teflon from the etch process. Finally, the test structures were released by vapor phase HF etching (VPE-200, Idonus) of sacrificial layer.

The scalloping shape and asperity size of sidewall surfaces are varied by changing the DRIE process parameters. In this article, two different DRIE process parameters were adopted to etch silicon layer and etch parameters are shown in Table. I. In the DRIE-I process, continuous etch and passivation cycles are performed with 5 sec and 2 sec respectively, whereas in the DRIE-II process, the etch cycle time reduced to 1.5 sec (with ramping) to obtain smaller asperity size. The scanning electron microscope (SEM) images of fabricated test structures is shown in Fig. 4.

V. RESULTS AND DISCUSSIONS

The fabricated test structures were tested in a cleanroom (Class 100, 20°C, 40% humidity). The testing equipment composed of a power supply system, microscope, a high-speed camera (Plexlogger-PL3 series, Shinano Kenshi) for image acquisition, and a data acquisition system, as shown in Fig. 5. The power supply system in this experiment offers two sets of driving voltages. One is applied to the normal actuator to produce a normal force on the contact surfaces, and the other is operated on a tangential actuator to initiate frictional motion. Fig. 6 shows SEM images of test structure sidewall surfaces fabricated with DRIE-I and DRIE-II process parameters. The scallop dimensions of DRIE-I and DRIE-II sidewall surfaces were extracted through SEM, whose values are around 650 nm and 280 nm, respectively. Fig. 7 shows the optical image of a contact pair which brought into contact by applying DC voltage ($V_n = V_a = 20$V) on a normal actuator to study the frictional behavior on the DRIE sidewall surfaces.
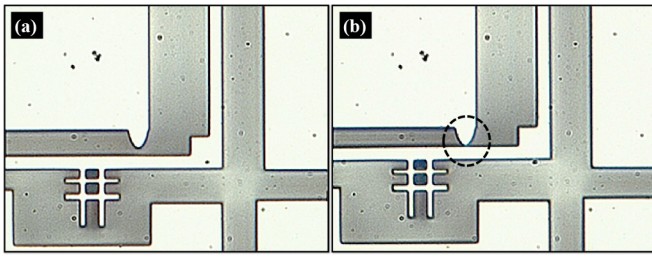
Fig. 7. Optical microscope image of contact pair (a) before and (b) after applying voltage ($V_n = V_a$) on normal comb actuator to bring the contact pair surfaces into contact.
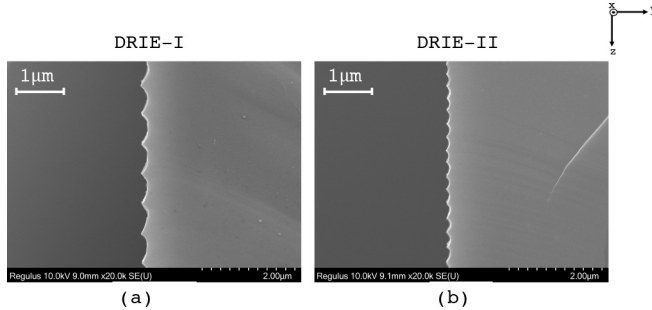

Fig. 8. SEM image of test structure sidewall profiles fabricated with (a) DRIE-I and (b) DRIE-II process.

During the experiment, image patterns of test structure were captured through the high-speed camera (50 frames per second) in corresponding with the applied voltages V_t and V_n. The working frequency of waveform (ramping voltage on actuators) is limited to low range, i.e., 1V/sec, to obtain a better acquisition accuracy. Because of the relatively low speed, damping effects due to air resistance were neglected on the actuator. The relative motion of the contact pairs during the experiments was obtained by using image processing software (PLEXLOGplusII application, which came along with the high-speed camera). In the DRIE process, due to the alternating operations of etching and passivation cycles, nearly sinusoidal ridges (scallops) were formed on the sidewall surfaces along a direction perpendicular to the depth of the silicon wafer as shown in Fig. 8. In each DRIE process, considering the two contacting sidewall surfaces were fabricated in the same process with synchronized etching and passivation cycles, peak-to-peak contact between the two sidewall surfaces would occur, as shown in Fig. 9 and the detailed scallop dimensions of DRIE-I and DRIE-II fabricated test structures are mentioned in Fig. 9.

Fig. 10 shows the relative displacement of contacting surface pair with the driving voltage (V_t) applying on tangential arm under different normal holding voltage (V_n) on a normal arm. At the driving voltage $V_t = V_{cri}$, the contact beam (tangential arm) starts slipping where the electrostatic force on the tangential comb actuator overcomes the restoring force caused by suspended beams and extended beam that connected to the tangential arm and also the maximum static frictional force acting between the contact pair. From Fig. 10, it shows that with the increment of normal voltage V_n on the contact pair, V_{cri} increased correspondingly to overcome the
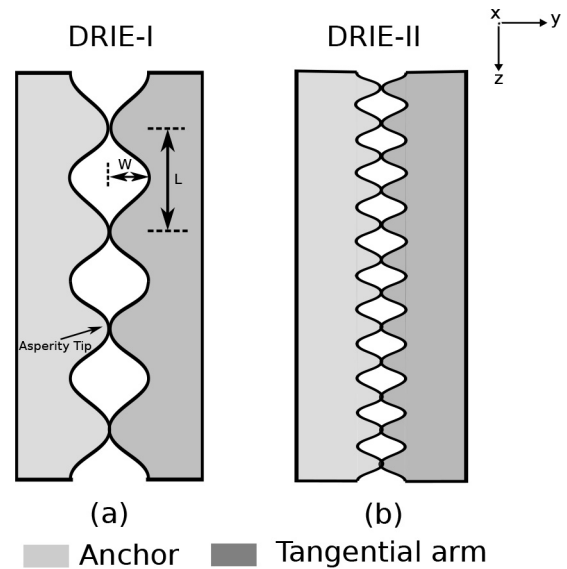

Fig. 9. Schematic diagram of the contact region with peak-to-peak contact at the sidewall surfaces (a) Test structure sidewall profile of DRIE-I process where L = 650 nm, W = 270 nm and asperity tip diameter = 50 nm (b) Test structure sidewall profile of DRIE-II process where L = 280 nm, W = 80 nm and asperity tip diameter = 35 nm.
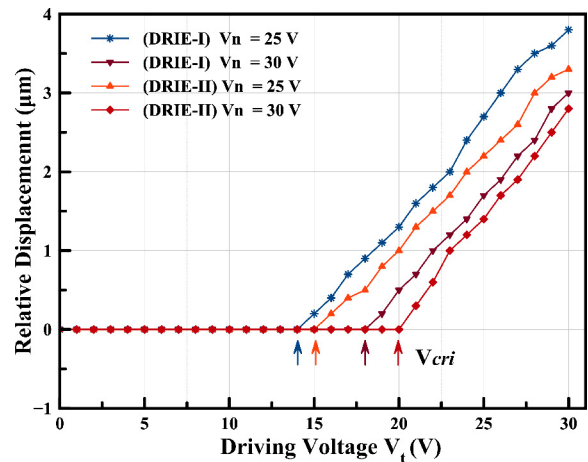

Fig. 10. Shows the relative displacement of contacting surface pair with the increment of driving voltage (V_t) under different normal holding voltage (V_n) of two different DRIE process parameter test structures and voltage V_{cri} is the point at which motion starts between contact pair, and the ↑ denotes voltage V_{cri} on the tangential arm for each test condition.

additional load experience on the contact sidewall surfaces. It is known that friction is generated by molecular adhesion such as van der Walls force and capillary force between the contact surfaces [16], [18], and the interlocking asperities on two surfaces [17]. As the asperities start interacting, friction force increases due to interlocking effects, adhesion forces, and the normal load on contact surfaces. The real contact area between the contact surfaces depends on the roughness (asperity size) and normal load, as shown in Fig. 9. From Fig. 10, it is clearly evident that V_{cri} is higher for DRIE-II than DRIE-I surfaces since the real contact area between the frictional pair of DRIE-II is higher than the DRIE-I for corresponding normal loads due to their asperity size difference on sidewall surfaces.
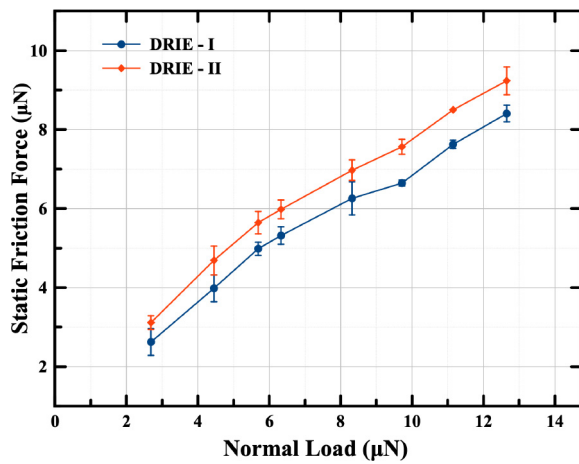
Fig. 11. Shows the static friction force versus normal load on contacting surfaces for the two DRIE test structures.
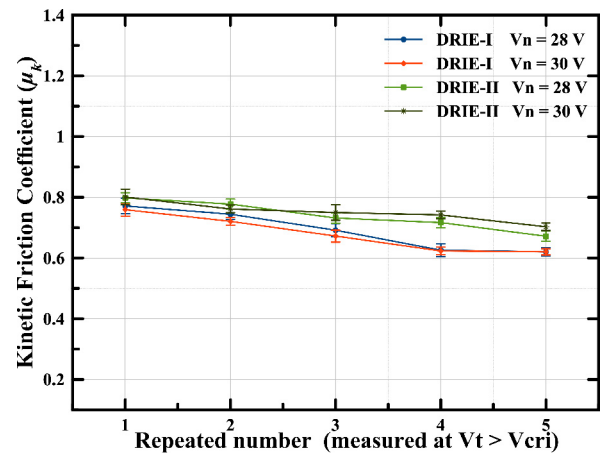

Fig. 12. Shows the static friction coefficient μ_s versus normal load on contacting surfaces for the two DRIE test structures.

Fig. 13. Shows the dynamic friction coefficient (μ_k) measured at different driving voltages ($V_t > V_{cri}$) on sidewall surface of two test structures at different normal holding voltage (V_n).
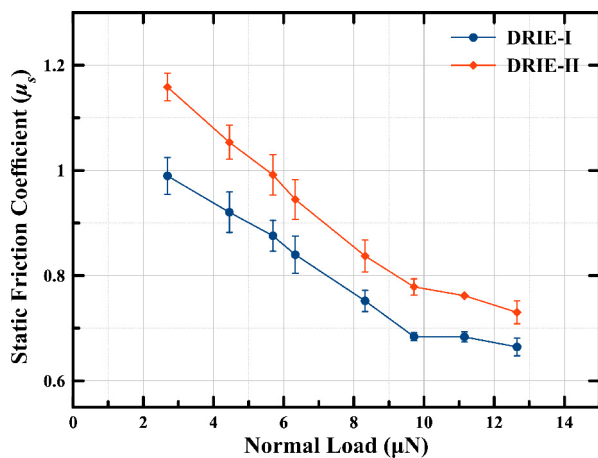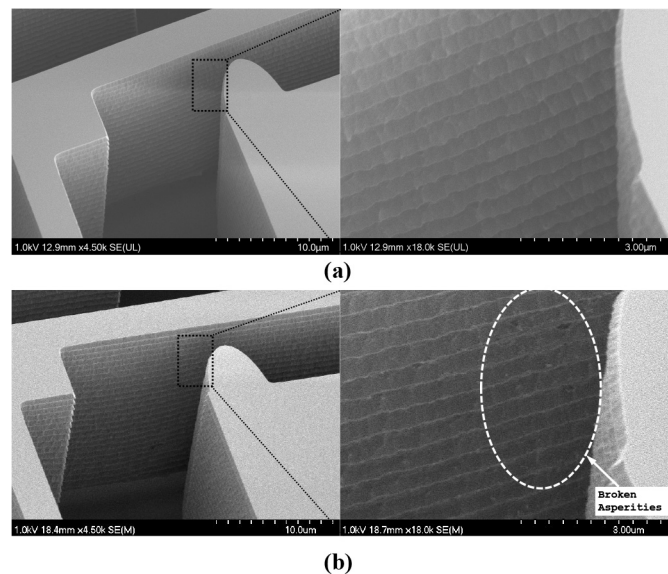

Fig. 14. SEM image of sidewall contact surface of DRIE-I test structures under wear experiments (a) before and (b) after testing (10000 cycles), where broken asperities can clearly seen on the enlarged surface.

For each test condition, the experiment was repeated at least five times to obtain a more accurate result from the test structures. The error bar of each point indicates one standard deviation above and below the corresponding average value. Fig. 11 shows the influence of static friction force with increasing normal load (μN) on the sidewall surfaces of the contact pair and Fig. 12 shows the static friction coefficient (μ_s) of DRIE sidewall surfaces with an increase in normal load. At low normal load, higher μ_s is observed where the van der Walls and capillary forces become significant, and with the increase in normal load, these Vander walls and capillary forces become secondary compared to the external force. DRIE-II process test structures experience a slightly higher static friction coefficient (μ_s) than the DRIE-I process structures due to their asperity size, which leads to a different contact area. The measured coefficient of static friction exhibits nonlinear dependence on the applied normal load.

Fig. 13 shows the dynamic friction coefficient (μ_k) on sidewall surfaces, which are measured at different driving voltages ($V_t > V_{cri}$) once the contact surface pair starts slipping under certain holding voltages (V_n) on the normal arm. It shows that normal forces may have less effect on dynamic friction

coefficient (μ_k) than the static friction coefficient (μ_s) on both the DRIE process, however DRIE-II process experiences a slightly higher dynamic friction coefficient than the DRIE-I due to their asperity size difference. Average measured values of the dynamic friction coefficient of DRIE-I and DRIE-II test structures for the first few cycles are 0.64±0.03, 0.72±0.04 respectively.

Wear experiments were carried on the test structure to determine the change of friction coefficients with the accumulation of wear cycles. For the wear analysis, DRIE-I process test structures were adopted and repetitive tests were performed on the contact pair by applying a voltage $V_n = 25V$ on normal comb actuator. The biased sine driving voltage applied on the tangential actuator, which is used to initiate reciprocation between the contact pair. The friction coefficient (μ_k) of contact pairs were evaluated at regular intervals during the wear experiments. The contact surfaces on the test structures were
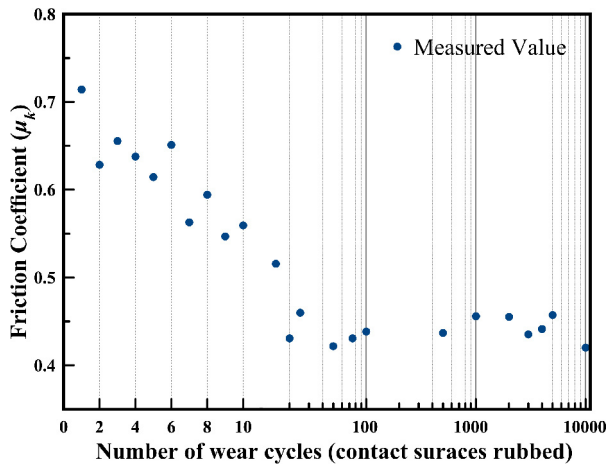
Fig. 15. Shows the friction coefficient (μ) versus cycle number at V_n=25V (number of times contact surfaces rubbed each other).

examined after the experiments to see the evidence of wear. Fig. 14 shows the sidewall contact surfaces of test structures before, and after the experiment, in this case, contact rubbed against one another for 10000 cycles before examine. There is a clear delineation between the area of the sidewall subjected to the sliding contact and the adjacent area not contacted (see Fig. 14b).

Fig. 15 shows the change of the friction coefficient of the contact surface versus the number of wear cycles. The obtained result shows that the friction coefficient has a very high initial value, then it drops with each subsequent cycle for a few cycles and finally reaches steady-state value. It implies that as the surfaces rub against one another, some asperities are broken off, and the surface roughness decreases each time until nearly all asperities above critical size are gone. After this point, the roughness stays relatively constant and the friction coefficient does not change very much. The final steady-state value of the friction coefficient is 0.44±0.01. From the results, it suggests that contact surfaces of MEMS devices should be conditioned before use by putting the sliding surfaces through several cycles (for the fabricated devices, 20–25 cycles was found to be enough), which ensures that the friction coefficient remains constant through the devices lifetime provided with proper encapsulation. It is worth mentioning that, in practice, the DRIE etched sidewalls have a slightly negative etch angle, so only partial contact would occur between the two sidewall surfaces when they brought in contact. More detail analysis of sidewall surface friction behavior on the DRIE etching profile angle would be an exciting topic for future exploration.

VI. CONCLUSION

An on-chip test structure with two orthogonally placed comb-drive actuators was designed and fabricated to study the frictional behavior of DRIE etched sidewall surfaces of silicon micromachined structures. The static and dynamic friction coefficients of DRIE sidewall surfaces were studied under the influence of normal load with different DRIE process parameters. Experiment results indicate that with the increment of normal load on the contacting pair, static friction is no longer a constant value, and it exhibits a nonlinear dependence. However, the normal load has less influence on the dynamic friction coefficient on sidewall surfaces. Through experiments, it is evident that the DRIE process parameters (i.e., scalloping size) have a significant influence on friction coefficients, and variation in asperity size changes the real contact area between the contact pairs during their operation. From the wear analysis, it is found that the friction coefficient has a very high initial value, then it drops with each subsequent cycle for a few cycles due to the wear of asperities on the contact surfaces and finally reaches steady-state value. An easy-to fabricate, on-chip microinstrument reported in this paper can be potentially used to systematically investigate the effect of friction and wear characteristics of different sidewall surfaces.

REFERENCES

[1] N. Maluf, "An introduction to microelectromechanical systems engineering," *Meas. Sci. Technol.*, vol. 13, no. 2, pp. 229–229, Jan. 2002.

[2] R. Ghodssi and P. Lin, *MEMS Materials and Process Handbook*. New York, NY, USA: Springer, 2011.

[3] P. H. Pham, K. T. Nguyen, and L. B. Dang, "Design and performance of a high loading electrostatic micro linear motor," *Microsyst. Technol.*, vol. 21, no. 11, pp. 2469–2474, Nov. 2015.

[4] W.-M. Zhang and G. Meng, "Friction and wear study of the hemispherical rotor bushing in a variable capacitance micromotor," *Microsyst. Technol.*, vol. 12, no. 4, pp. 283–292, Mar. 2006.

[5] R. R. Reddy, K. Komeda, Y. Okamoto, E. Lebrasseur, A. Higo, and Y. Mita, "A zero-power sensing MEMS shock sensor with a latch-reset mechanism for multi-threshold events monitoring," *Sensors Actuators A Phys.*, vol. 295, pp. 1–10, Aug. 2019.

[6] A. Attaran and R. Rashidzadeh, "Ultra low actuation voltage RF MEMS switch," *Micro Nano Syst. Lett.*, vol. 3, no. 1, p. 7, Aug. 2015.

[7] R. Yeh, S. Hollar, and K. S. J. Pister, "Single mask, large force, and large displacement electrostatic linear inchworm motors," *J. Microelectromech. Syst.*, vol. 11, no. 4, pp. 330–336, Aug. 2002.

[8] S. K. Sinha, N. Satyanarayana, and S. C. Lim, *Nano-Tribology and Materials in MEMS*. Heidelberg, Germany: Springer, 2013.

[9] J. Walraven, "Failure mechanisms in MEMS," in *Proc. ITC Int. Test Conf.*, 2004, pp. 828–833.

[10] P. Decuzzi and D. J. Srolovitz, "Scaling laws for opening partially adhered contacts in MEMS," *J. Microelectromech. Syst.*, vol. 13, no. 2, pp. 377–385, Apr. 2004.

[11] R. Maboudian, W. R. Ashurst, and C. Carraro, "Tribological challenges in micromechanical systems," *Tribology Lett.*, vol. 12, no. 2, pp. 95–100, Feb. 2002.

[12] W. M. van Spengen, "Hints of atomic scale phenomena in adhesion and friction measurements with MEMS devices," *Tribology Mater. Surfaces Interfaces*, vol. 4, no. 3, pp. 115–120, 2010.

[13] D. M. Tanner *et al.*, "MEMS reliability: Infrastructure, test structures, experiments, and failure modes," Sandia Nat. Lab., U.S. Dept. Energy, Albuquerque, NM, USA, Rep. SAND2000-0091, 2000.

[14] N. R. Tas, C. Gui, and M. Elwenspoek, "Static friction in elastic adhesion contacts in MEMS," *J. Adhesion Sci. Technol.*, vol. 17, no. 4, pp. 547–561, 2003.

[15] D. H. Alsem, R. Van Der Hulst, E. A. Stach, M. T. Dugger, J. T. M. De Hosson, and R. O. Ritchie, "Wear mechanisms and friction parameters for sliding wear of micron-scale polysilicon sidewalls," *Sensors Actuators A Phys.*, vol. 163, no. 1, pp. 373–382, 2010.

[16] M. Wautelet, "Scaling laws in the macro-, micro- and nanoworlds," *Eur. J. Phys.*, vol. 22, no. 6, pp. 601–611, Oct. 2001.

[17] M. Nosonovsky and B. Bhushan, "Scale effect in dry friction during multiple-asperity contact," *J. Tribology*, vol. 127, no. 1, pp. 37–46, Feb. 2005.

[18] Y. Mo, K. T. Turner, and I. Szlufarska, "Friction laws at the nanoscale," *Nature*, vol. 457, no. 7233, pp. 1116–1119, 2009.

[19] Z. Guo, Z. Feng, S. Fan, D. Zheng, and H. Zhuang, "Research development of measuring methods on the tribology characters for movable MEMS devices: A review," *Microsyst. Technol.*, vol. 15, no. 3, pp. 343–354, Mar. 2009.

[20] K. Komvopoulos, "Adhesion and friction forces in microelectromechanical systems: Mechanisms, measurement, surface modification techniques, and Adhesion theory," *J. Adhesion Sci. Technol.*, vol. 17, no. 4, pp. 477–517, 2003.

[21] P. Stoyanov and R. R. Chromik, "Scaling effects on materials tribology: From macro to micro scale," *Materials*, vol. 10, no. 5, p. 550, 2017.

[22] B. Bhushan and C. Dandavate, "Thin-film friction and adhesion studies using atomic force microscopy," *J. Appl. Phys.*, vol. 87, no. 3, pp. 1201–1210, 2000.

[23] E.-S. Yoon, R. A. Singh, H.-J. Oh, and H. Kong, "The effect of contact area on nano/micro-scale friction," in *Proc.15th Int. Conf. Wear Mater.*, vol. 259, no. 7, 2005, pp. 1424–1431.

[24] F. Buja, G. Fiorentino, J. Kokorian, and W. M. van Spengen, "Observation of nanoscale adhesion, friction and wear between ALD al2o3coated silicon MEMS sidewalls," *Nanotechnology*, vol. 26, no. 25, May 2015, Art. no. 255701.

[25] W. M. van Spengen and J. W. M. Frenken, "The leiden MEMS tribometer: Real time dynamic friction loop measurements with an on-chip tribometer," *Tribology Lett.*, vol. 28, no. 2, pp. 149–156, Nov. 2007.

[26] S. J. Timpe and K. Komvopoulos, "An experimental study of sidewall adhesion in microelectromechanical systems," *J. Microelectromech. Syst.*, vol. 14, no. 6, pp. 1356–1363, Dec. 2005.

[27] D. C. Senft and M. T. Dugger, "Friction and wear in surface micromachined tribological test devices," in *Proc. SPIE*, vol. 3224, 1997, pp. 31–38.

[28] W. R. Ashurst, M. de Boer, C. Carraro, and R. Maboudian, "An investigation of sidewall adhesion in MEMS," in *Proc. 11th Int. Conf. Solid Films Surfaces Appl. Surface Sci.*, vols. 212–213, 2003, pp. 735–741.

[29] S. J. Timpe and K. Komvopoulos, "The effect of adhesion on the static friction properties of sidewall contact interfaces of microelectromechanical devices," *J. Microelectromech. Syst.*, vol. 15, no. 6, pp. 1612–1621, Dec. 2006.

[30] I. H. Hwang, Y. G. Lee, and J. H. Lee, "A micromachined friction meter for silicon sidewalls with consideration of contact surface shape," *J. Micromech. Microeng.*, vol. 16, no. 11, pp. 2475–2481, 2006.

[31] J. Wu, S. Wang, and J. Miao, "A MEMS device for studying the friction behavior of micromachined sidewall surfaces," *J. Microelectromech. Syst.*, vol. 17, no. 4, pp. 921–933, 2008.

[32] Z. Guo, Y. Meng, C. Su, and H. Wu, "An on-chip micro-friction tester for tribology research of silicon based MEMS devices," *Microsyst. Technol.*, vol. 14, no. 1, pp. 109–118, 2008.

[33] D. H. Alsem, M. T. Dugger, E. A. Stach, and R. O. Ritchie, "Micronscale friction and sliding wear of polycrystalline silicon thin structural films in ambient air," *J. Microelectromech. Syst.*, vol. 17, no. 5, pp. 1144–1154, Oct. 2008.

[34] J. Wu, S. Wang, and J. Miao, "Friction characteristics of the curved sidewall surfaces of a rotary MEMS device in oscillating motion," *J. Micromech. Microeng.*, vol. 19, no. 6, 2009, Art. no. 065020.

[35] H. Yu, G. Zhou, S. K. Sinha, J. Y. Leong, and F. S. Chau, "Characterization and reduction of MEMS sidewall friction using novel microtribometer and localized lubrication method," *J. Microelectromech. Syst.*, vol. 20, no. 4, pp. 991–1000, Aug. 2011.

[36] N. Ansari and W. R. Ashurst, "Single-crystal-silicon-based microinstrument to study friction and wear at MEMS sidewall interfaces," *J. Micromech. Microeng.*, vol. 22, no. 2, 2012, Art. no. 025008.

[37] A. Gkouzou, J. Kokorian, G. C. A. M. Janssen, and W. M. van Spengen, "Friction and dynamically dissipated energy dependence on temperature in polycrystalline silicon MEMS devices," *Microsyst. Technol.*, vol. 24, no. 4, pp. 1899–1907, Apr. 2018.

[38] R. Legtenberg, A. W. Groeneveld, and M. Elwenspoek, "Comb-drive actuators for large displacements," *J. Micromech. Microeng.*, vol. 6, no. 3, pp. 320–329, 1999.

[39] R. R. Reddy, Y. Okamoto, and Y. Mita, "An on-chip test structure for studying the frictional behavior of deep-RIE MEMS sidewall surfaces," in *Proc. IEEE Int. Conf. Microelectron. Test Struct.*, 2018, pp. 4–9.

[40] F. Laerme, A. Schilp, K. Funk, and M. Offenberg, "Bosch deep silicon etching: Improving uniformity and etch rate for advanced MEMS applications," in *12th IEEE Int. Conf. Tech. Dig. Micro Electro Mech. Syst. (MEMS)*, Jan. 1999, pp. 211–216.